The Impact of Acceptor-Acceptor Homocoupling on the Optoelectronic Properties and Photovoltaic Performance of PDTSQx(ff) Low Bandgap Polymers

Peer-reviewed author version

PIROTTE, Geert; KESTERS, Jurgen; CARDEYNAELS, Tom; VERSTAPPEN, Pieter; D'HAEN, Jan; LUTSEN, Laurence; Champagne, Benoit; VANDERZANDE, Dirk & MAES, Wouter (2018) The Impact of Acceptor-Acceptor Homocoupling on the Optoelectronic Properties and Photovoltaic Performance of PDTSQx(ff) Low Bandgap Polymers. In: MACROMOLECULAR RAPID COMMUNICATIONS, 39(14) (Art N° 1800086).

DOI: 10.1002/marc.201800086
Handle: http://hdl.handle.net/1942/27687

DOI: 10.1002/marc.((insert number))

Communication

The Impact of Acceptor-Acceptor Homocoupling on the Optoelectronic Properties and Photovoltaic Performance of PDTSQx$_{ff}$ Low Bandgap Polymers[a]

*Geert Pirotte, Jurgen Kesters, Tom Cardeynaels, Pieter Verstappen, Jan D'Haen, Laurence Lutsen, Benoît Champagne, Dirk Vanderzande, and Wouter Maes**

_____

Dr. Geert Pirotte, Dr. Jurgen Kesters, Tom Cardeynaels, Dr. Pieter Verstappen, Prof. Jan D'Haen, Prof. Dirk Vanderzande, Prof. Wouter Maes

UHasselt – Hasselt University, Institute for Materials Research (IMO-IMOMEC), Design & Synthesis of Organic Semiconductors (DSOS) – Electrical and Physical Characterization (ELPHYC)

Agoralaan – Building D, 3590 Diepenbeek, Belgium

E-mail: wouter.maes@uhasselt.be

Tom Cardeynaels, Prof. Benoît Champagne

Laboratory of Theoretical Chemistry, Theoretical and Structural Physical Chemistry Unit, Namur Institute of Structured Matter, University of Namur

Rue de Bruxelles 61, 5000 Namur, Belgium

Prof. Jan D'Haen, Dr. Laurence Lutsen, Prof. Dirk Vanderzande, Prof. Wouter Maes

IMEC - IMOMEC

Universitaire Campus – Wetenschapspark 1, 3590 Diepenbeek, Belgium

[a] **Supporting Information** is available online from the Wiley Online Library or from the author.

Push-pull type conjugated polymers applied in organic electronics do not always contain a perfect alternation of donor and acceptor building blocks. Miss-couplings can occur, which have a noticeable effect on the device performance. In this work, the influence of homocoupling on the optoelectronic properties and photovoltaic performance of PDTSQx$_{ff}$ polymers is investigated, with a specific focus on the quinoxaline acceptor moieties. A homocoupled biquinoxaline segment is intentionally inserted in specific ratios during the polymerization. These homocoupled units cause a gradually blue-shifted absorption, while the HOMO energy levels decrease only significantly upon the presence of 75 to 100% of homocouplings. DFT calculations show that the homocoupled acceptor unit generates a twist in the polymer backbone, which leads to a decreased conjugation length and a reduced aggregation tendency. The virtually defect-free PDTSQx$_{ff}$ affords a solar cell efficiency of 5.4%, which only decreases strongly upon incorporating a homocoupling degree over 50%.

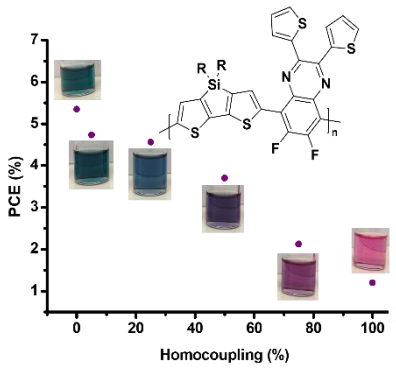

1 Introduction

Over the past two decades, bulk heterojunction (BHJ) organic photovoltaic (OPV) devices evolved into attractive candidates for renewable energy production.[1,2] This organic thin-film PV technology shows beneficial properties such as flexibility, tunable absorption profiles and printing ability, allowing low-cost large scale device fabrication. Multiple combinations of efficiently intermixed electron donor polymers and acceptors (fullerenes as well as non-fullerene alternatives) have been developed, affording power conversion efficiencies (PCEs) over 13% in solution processed single layer devices.[3–12] The state of the art electron donor polymers are push-pull type copolymers, consisting of alternating electron-rich (push or donor) and electron-poor (pull or acceptor), mainly heterocyclic, building blocks. These polymers are generally synthesized by palladium-catalyzed cross-coupling reactions (mainly Suzuki and Stille) of bifunctional monomers. Although frequently neglected, these reactions do not always provide the desired perfect alternation of push and pull building blocks. Even upon applying 'nearly perfect' conditions, e.g. an oxygen-free atmosphere and a proper Pd-ligand stoichiometry, homocoupling between either two organotin/boron or two arylhalide units can occur.[13–16] The importance and possible abundance of these miss-coupled structural units for the performance of organic solar cells has only recently been recognized and a few reports on this have appeared.[17–24]

By synthesizing a diketopyrrolopyrrole polymer (PDPPTPT) under different conditions, Janssen et al. in 2014 showed that the presence of homocoupling defects of the polymer donor unit causes a red-shift in the absorption spectrum.[22] It was further emphasized that homocoupling defects can lead to low-lying energy trap sites and they may effectively increase the HOMO and decrease the LUMO of the polymer. The main effects on the solar cell level were a decrease in photocurrent and a significantly lower PCE (dropping from 7.5 to 4.5%). Another polymer for which homocoupling defects were shown to be important, is the popular

material PTB7. In 2015, Vangerven and co-workers investigated several commercial batches of PTB7 by gel permeation chromatography (GPC) and matrix assisted laser desorption/ionization – time of flight (MALDI-TOF) mass spectrometry.[21] The lower molecular weight batches clearly showed a bimodal molecular weight distribution. Analysis by MALDI-TOF revealed that homocoupling occurred for both the brominated and stannylated monomers used in the Stille polycondensation. In agreement with the observations by Janssen et al., homocoupling also caused a clear red-shift in the absorption spectra and a significant drop in PCE (from 7.0 to 2.7%) for the resulting polymer solar cells. Apart from altering the HOMO and LUMO levels of the polymers, homocoupling can also cause changes in the aggregation behavior upon film formation, which is of crucial importance to achieve high efficiencies. Yu et al. reported similar effects of homocoupling on the performance of PTB7 polymer solar cells.[20] Additionally, it was identified that homocoupling leads to increased bimolecular recombination in the devices. In 2016, Sommer and co-workers reported on the occurrence of homocouplings in the PCDTBT polymer synthesized by Suzuki polycondensation. Up to 8% homocoupling of the carbazole unit was observed, leading to a strong decrease in short-circuit current density (J_{sc}).[17]

Although the reports are still limited, the presence of homocoupling in the donor polymer clearly has a strong influence on the photovoltaic performance. Characterization of the effect of homocoupling remains, however, a difficult task as it does not influence one parameter solemnly and the extent to which homocoupling occurs can differ from batch to batch. It also remains troublesome to precisely analyze and quantify the amount of homocoupling present. ^{1}H NMR analysis is often complicated due to significant signal broadening, although it is possible if (high temperature) NMR yields narrow signals.[25,26] Nevertheless, there is certainly a need to further analyze the effects of homocoupling, preferentially for cases which allow proper characterization of the polymer backbone structure. Dithienosilole-quinoxaline

(PDTSQx) copolymers are perfectly suited for such studies as they show minimal signal broadening in ^{1}H NMR and can easily be analyzed by MALDI-TOF. Upon fluorination of the quinoxaline unit, average efficiencies up to 5% have been reached for the analogous PCPDTQx polymers.[27,28] In this study, PDTSQx$_{ff}$ was synthesized by Stille polycondensation between the stannylated dithienosilole and the brominated difluoroquinoxaline. PDTSQx$_{ff}$ has a high solubility in common organic solvents, allowing an easy characterization, and it affords a moderate solar cell efficiency of ~5.5%, which allows proper detection of fluctuations of the photovoltaic performance. PDTSQx$_{ff}$ can also easily be analyzed by MALDI-TOF up to molecular weights of 20 kDa to enable proper determination of the homocoupling content.[18,19,21]

Previous studies have mainly focused on the influence of homocoupling of the donor unit, although it has been shown that homocoupling in the acceptor unit also readily occurs,[29] and in a rare case even improved the photovoltaic performance.[30] For this reason, the acceptor unit was specifically targeted in the present study. A homocoupled biquinoxaline acceptor is synthesized and added to the polymerization reaction. Effective built-in of this building block is confirmed by MALDI-TOF and ^{1}H NMR. The impact of acceptor-acceptor homocoupling on the photovoltaic performance is analyzed and correlated to the gradually changing physical and optoelectronic material properties.

2 Results and Discussion

To mimic homocoupling, the quinoxaline monomer was deliberately homocoupled prior to polymerization (**Scheme 1**). Br-(Qx$_{ff}$)$_2$-Br can be synthesized directly from the standard Br-Qx$_{ff}$-Br monomer by reaction with hexabutylditin under Stille conditions. Although only 0.4 equivalents of hexabutylditin were added to favor dimer formation, the reaction mixture consisted of a distribution of oligomers, ranging from monomers to pentamers. The different

oligomers were separated by recycling preparative size-exclusion chromatography (prep-SEC) to yield the pure dibrominated diquinoxaline. Despite the low yield, this method was more effective than other direct coupling methods such as $Ni(COD)_2$, which also yielded a large portion of debrominated products, hindering purification. To assure proper polymerization, the Me_3Sn-DTS-$SnMe_3$ monomer was used directly after purification (removal of the monostannylated compound) with prep-SEC.

Specific quantities of the quinoxaline dimer – 0, 5, 25, 50, 75 and 100% with respect to the standard Qx monomer – were then added to the polymerization reaction. After the reactions, Pd was removed by the addition of sodium diethyldithiocarbamate trihydrate and precipitation in methanol. The resulting polymers were further purified by prep-SEC, which also allowed tuning of the number-average molecular weight (M_n). As large differences in molecular weight could also cause differences in the optoelectronic properties and morphology of the BHJ solid state blend, the molecular weight of all samples was tuned between 25 and 30 kDa (**Table 1**).

MALDI-TOF was then used to confirm the amount of homocouplings along the polymer chain and for determination of the polymer end groups (Figure S1-S10). For **P1**, molecular weights up to 20 kDa could be observed and no clear signals of homocoupling segments were found (**Figure 1**). The end groups were mainly methyl groups or a combination of one hydrogen and one methyl, independent of the amount of homocoupling. End group determination is most easily done in the lower molecular weight region as the resolution goes down with increasing molecular weight. The methyl end groups are likely the result of a methyl-shift originating from the trimethylstannyl functionalities.[31] Methyl end groups are rather found on the Qx polymer chain ends and hydrogen groups on the DTS ends. Careful analysis of the MALDI-TOF mass spectrum of the lower molecular weight fraction of **P4** (**Figure 2**) shows a distribution of polymer chain lengths with different Qx:DTS ratios, which on average match the projected percentage of homocoupling, confirming successful polymerization and effective built-in of the

Qx dimer. A similar overall analysis can be made for the MALDI-TOF mass spectra of the other PDTSQx$_{ff}$ polymers with different homocoupling content (Figure S1-S10). The gradual increase of homocoupling units was also apparent from the ^{1}H NMR spectra (Figure S15-S20).

The polymers were also characterized by UV-VIS absorption spectroscopy in solution and thin film (**Figure 3**). A small percentage of homocoupling (5%) does not significantly change the absorption profile of the polymer, while the presence of larger amounts clearly causes a blue-shift of the absorption maximum (Table 1) and alters the color of the polymer in solution (Figure S21). The blue-shift is most pronounced when comparing 0-25, 25-50 and 50-75% of homocoupling, whereas increasing the homocoupling content from 75 to 100% only changes the width of the absorption band. Very similar observations were made for the solid state spectra. Additionally, the virtually defect-free polymer has a clear red-shifted shoulder in the absorption spectrum which can be attributed to aggregation. A diminishing presence of this shoulder across the polymer series indicates that homocoupling significantly decreases the tendency to aggregate, even at low concentrations (5%).

Determination of the oxidation/reduction potentials and the derived frontier orbital energy levels was done by performing cyclic voltammetry (CV) on thin films of the polymer samples (Figure S23-S28). The obtained values (Table 1) show that the LUMO energy level of the pristine PDTSQx$_{ff}$ polymer is barely affected by the presence of homocoupling. The HOMO levels remain more or less constant up to 50% homocoupling and significant differences were only detected for the 75% and pure homocoupled polymers. Comparison of the HOMO and LUMO energy levels of Br-Qx$_{ff}$-Br (-6.26 eV and -3.50 eV) and Br-(Qx$_{ff}$)$_2$-Br (-6.26 eV and -3.46 eV) indicates that the acceptor strength remains similar upon dimerization of the Qx monomer.

The blue-shift in the UV-VIS spectra and the stabilization of the HOMO level (from CV) seem to point to a disruption of the conjugation in the polymer backbone upon homocoupling. The change in conjugation becomes apparent at homocoupling levels of around 50% and higher, illustrating that the amount of homocoupling needed to effectively disturb the conjugation length is quite high. To further unravel the influence of homocoupling on the backbone conjugation, DFT calculations were performed using the M06 exchange-correlation functional and the 6-311G(d) basis set.[32] All calculations were carried out using Gaussian09.[33] First, the ground state geometries were optimized for the individual donor and acceptor moieties, the donor-acceptor combinations (DA) and acceptor-acceptor (AA) homocoupled moieties. The alkyl chains were replaced with methyl groups to facilitate the calculations without changing the electronic properties of the oligomers. Several conformations for the donor and acceptor units have been considered and the calculations were performed using the most stable conformers (Figure S29 and Table S1). From the geometry optimizations for both the AA homocoupled units and the polymers containing 50% and 100% homocoupling (Figure S29-S31), a large dihedral angle between the adjacent acceptor units of around 57° is observed. The insertion of a homocoupled acceptor unit therefore causes a deviation from planarity, which will significantly lower the ability of the polymer chains to aggregate upon film formation. Within the same polymer chain, this deviation results in a decrease of orbital overlap and therefore in a decrease in conjugation. This is also apparent from the obtained orbital topologies (Figure S32) in which it is clear that upon increasing level of homocoupling, the HOMO is more localized on the DTS units instead of the entire backbone, whereas the LUMO level remains largely unchanged. Time-dependent density functional theory (TD-DFT) calculations using the M06 exchange-correlation functional and the 6-311G(d) basis set, and taking into account the solvent (chloroform) effects using the polarizable continuum model, were performed to simulate the absorption spectra of polymers containing 0, 50 and 100%

homocoupling (Figure S33). These simulated spectra show a blue-shift with increasing homocoupling percentage, in line with the experimental observations. The calculations also confirm a stabilization of the HOMO level, while the LUMO remains constant.

Photovoltaic devices were then finally prepared to investigate the influence of homocoupling on the solar cell parameters (**Table 2** and **Figure 4**). The virtually defect-free PDTSQx$_{ff}$ polymer **P1** shows the highest performance (average PCE of 5.43%), with a downward trend toward higher homocoupling contents (1.50% for **P6**). Even though the J_{sc} perfectly follows this trend, a decrease in fill factor (FF) can be observed starting from 50% homocoupling. Furthermore, the open-circuit voltage (V_{oc}) also increases up to this point, corresponding to the observed changes in HOMO energy level. The external quantum efficiency (EQE) spectra, shown in Figure 4, indicate that up to 50% homocoupling, the decrease in J_{sc} can mostly be ascribed to optical effects (blue-shift in UV-VIS), whereas upon higher contents of homocoupling, the electronic properties are also affected more strongly, lowering the EQE over the entire wavelength range. Atomic force microscopy (AFM) images (Figure S34) show a similar roughness for all blended films, and transmission electron microscopy (TEM) images (Figure S35) show identical morphologies for all active layer blends, overruling the idea that the loss in FF could be ascribed to (major) changes in morphology. Finally, hole-only devices were fabricated with the ITO/PEDOT:PSS/active layer/Au configuration to investigate the electronic properties in the devices. Space charge limited current regimes could be identified for **P1**-**P5** (Figure S36), showing a decrease in hole mobility upon increasing the homocoupling content, most likely due to a loss in polymer aggregation as observed in the UV-VIS spectra.

3 Conclusions

A well-defined amount of homocoupled quinoxaline acceptor monomer has gradually been built in in the photovoltaic polymer PDTSQx$_{ff}$, as confirmed by MALDI-TOF and ^{1}H NMR.

Rather than immediately affecting the electronic properties of the polymer, acceptor-acceptor homocoupling initially altered the optical response by decreasing the conjugation length due to a distortion of the polymer backbone planarity. This was mainly translated in a blue-shifted UV-VIS absorption spectrum and a decreased aggregation tendency. As the homocoupling content increased to 50% or more, also the electronic properties of the polymer were strongly affected, leading to a decrease in photocurrent and fill factor in the resulting polymer solar cells. As such, this study illustrates once again the importance of avoiding homocoupling in push-pull conjugated polymers to achieve optimal performance. Depending on the system, the tolerance to homocoupling defects may be different. In this particular case, the occurrence of acceptor-acceptor homocoupling is clearly identifiable by the color change, but in many other cases these defects may be more hidden and more careful analysis will be required. Current efforts in our group are directed toward efficient ways to avoid homocoupling.

4 Experimental Section

4.1 Materials and Methods

All reagents and chemicals were obtained from commercial sources and used without further purification. Solvents were dried by a solvent purification system (MBraun, MB-SPS-800) equipped with alumina columns. 4,4-Bis(2-ethylhexyl)-2,6-bis(trimethylstannyl)-4*H*-silolo[3,2-*b*:4,5-*b*']dithiophene[34] and 5,8-dibromo-6,7-difluoro-2,3-di(thiophen-2-yl)quinoxaline[28] were synthesized according to literature procedures. Preparative (recycling) size exclusion chromatography was performed on a JAI LC-9110 NEXT system equipped with JAIGEL 1*H* and 2*H* columns (eluent $CHCl_3$, flow rate 3.5 mL min^{-1}). ^1H NMR spectra were recorded in $CDCl_3$ or CD_2Cl_2 and chemical shifts (δ, in ppm) were determined relative to the residual $CHCl_3$ (7.26 ppm) or CD_2Cl_2 (5.32 ppm) absorption. The ^{13}C NMR spectrum of Br-$(Qx_{ff})_2$-Br was recorded in d_8-THF and chemical shifts were determined relative to the residual

THF (67.21 and 25.31 ppm) signals. High resolution electrospray ionization mass spectrometry (ESI-MS) was performed using an LTQ Orbitrap Velos Pro mass spectrometer equipped with an atmospheric pressure ionization source operating in the nebulizer assisted electrospray mode. The instrument was calibrated in the *m/z* range 220−2000 using a standard solution containing caffeine, MRFA and Ultramark 1621. MALDI-TOF mass spectra were recorded on a Bruker Daltonics Ultraflex II Tof/Tof. 1 µL of the matrix solution (16 mg mL^{-1} DTCB (*trans*-2-[3-(4-*tert*-butylphenyl)-2-methyl-2-propenylidene]malononitrile) in $CHCl_3$) was spotted onto an MTP Anchorchip 600/384 MALDI plate. The spot was allowed to dry and 1 µL of the analyte solution (0.5 mg mL^{-1} in $CHCl_3$) was spotted on top of the matrix. UV-VIS measurements were performed on a VARIAN Cary 500 UV-VIS-NIR spectrophotometer at a scan rate of 600 nm min^{-1}. The films for the UV-VIS measurements were prepared by drop casting a solution of the polymer in chloroform on a quartz substrate. The solid-state UV-VIS spectra were used to estimate the optical gaps (from the wavelength at the intersection of the tangent line drawn at the low energy side of the absorption spectrum with the x-axis: E_g (eV) = 1240/(wavelength in nm)). Electrochemical measurements (CV) were performed with an Eco Chemie Autolab PGSTAT 30 potentiostat/galvanostat using a three-electrode microcell with a platinum working electrode, a platinum counter electrode and a $Ag/AgNO_3$ reference electrode (silver wire dipped in a solution of 0.01 M $AgNO_3$ and 0.1 M NBu_4PF_6 in anhydrous acetonitrile). The reference electrode was calibrated against ferrocene/ferrocenium as an external standard. Samples were prepared by dip coating the platinum working electrode in the respective monomer/polymer solutions (also used for the solid-state UV-VIS measurements). The CV measurements were done on the resulting films with 0.1 M NBu_4PF_6 in anhydrous acetonitrile as electrolyte solution. To prevent air from entering the system, the experiments were carried out under a curtain of argon. Cyclic voltammograms were recorded at a scan rate of 100 mV s^{-1}. For the conversion of V to eV, the onset potentials of the first oxidation/reduction peaks were used and

referenced to ferrocene/ferrocenium, which has an ionization potential of −4.98 eV *vs.* vacuum. This correction factor is based on a value of 0.31 eV for Fc/Fc^+ *vs.* SCE[35] and a value of 4.68 eV for SCE *vs.* vacuum[36]: $E_{HOMO/LUMO}$ (eV) = −4.98 − $E_{onset\ ox/red}^{Ag/AgNO3}$ (V) + $E_{onset\ Fc/Fc+}^{Ag/AgNO3}$ (V). The reported values are the means of the first four redox cycles.

4.2 Synthetic Procedures

8,8'-Dibromo-6,6',7,7'-tetrafluoro-2,2',3,3'-tetra(thiophen-2-yl)-5,5'-biquinoxaline (Br-(Qx_{ff})$_2$-Br)

1,1,1,2,2,2-Hexabutyldistannane (1.72 g, 2.97 mmol), 5,8-dibromo-6,7-difluoro-2,3-di(thiophen-2-yl)quinoxaline (3.00 g, 6.15 mmol), $Pd_2(dba)_3$ (0.140 g, 0.15 mmol) and P(*o*-tol)$_3$ (0.187 g, 0.61 mmol) were dissolved in freshly degassed dry DMF (12 mL) and dry toluene (48 mL) under nitrogen atmosphere. The solution was purged with nitrogen for 30 min and heated to 100 °C for 20 h. The solution was then allowed to cool to room temperature and water was added. After extraction with chloroform, the organic layer was washed with brine, dried over $MgSO_4$, filtered and the solvent was removed under reduced pressure. The crude material was further purified by recycling prep-SEC and the pure compound was collected as a yellow solid (300 mg, 6%). ^{1}H NMR (400 MHz, $CDCl_3$, δ) 7.56 (dd, *J* = 5.0, 1.1 Hz, 2H), 7.44 (dd, *J* = 3.8, 1.1 Hz, 2H), 7.25 (dd, *J* = 5.1, 1.1 Hz, 2H), 7.19 (dd, *J* = 3.8, 1.1 Hz, 2H), 7.04 (dd, *J* = 5.0, 3.7 Hz, 2H), 6.86 (dd, *J* = 5.0, 3.8 Hz, 2H); ^{13}C NMR (100 MHz, THF-d_8, δ) 152.8 (dd, *J* = 37.6, 16.2 Hz), 150.3 (dd, *J* = 44.3, 16.5 Hz), 147.9, 147.6, 142.0, 137.0, 136.4, 132.4–127.6 (m), 116.7 (d, *J* = 11.2 Hz), 111.8 (d, *J* = 17.6 Hz); HRMS (ESI) *m/z*: $[M + H]^+$ calcd for $C_{32}H_{13}Br_2F_4N_4S_4$, 816.8306; found, 816.8253.

Polymerization

The appropriate amounts of 5,8-dibromo-6,7-difluoro-2,3-di(thiophen-2-yl)quinoxaline, 8,8'-dibromo-6,6',7,7'-tetrafluoro-2,2',3,3'-tetra(thiophen-2-yl)-5,5'-biquinoxaline and 4,4-bis(2-

ethylhexyl)-2,6-bis(trimethylstannyl)-4*H*-silolo[3,2-*b*:4,5-*b*']dithiophene, together with $Pd_2(dba)_3$ (3 mol%) and P(*o*-tol)$_3$ (12 mol%), were charged in a dry Schlenk tube equipped with a magnetic stirring bar. A freshly degassed mixture of dry DMF and toluene (2:8) was added, resulting in an overall monomer concentration of 110 mM. The reaction mixture was then stirred for 16 h at 110 °C. After cooling down to 70 °C, sodium diethyldithiocarbamate trihydrate (0.675 g, 2.99 mmol), dissolved in water (6 mL), was added and the mixture was stirred heavily for an additional 30 min. The organic phase was added to methanol, causing polymer precipitation, and the crude polymer material was collected by filtration and dried under reduced pressure. The polymer was further purified by recycling prep-SEC. Yield: **P1** = 73%, **P2** = 84%, **P3** = 66%, **P4** = 80%, **P5** = 84%, **P6** = 80%.

4.3 Photovoltaic Device Fabrication and Characterization

BHJ solar cells were prepared using the conventional architecture glass/ITO/PEDOT:PSS/**P1**-**P6**:$PC_{71}BM$/Ca/Al (or glass/ITO/PEDOT:PSS/ **P1**-**P6**:$PC_{71}BM$/Au in case of the hole-only devices). Prior to device processing, the ITO-coated substrates (100 nm, Kintec, sheet resistivity 20 Ω sq^{-1}) were subjected to a standard cleaning procedure using soap, demineralized water, acetone and isopropanol, followed by a UV/O_3 treatment for 15 min. PEDOT:PSS [poly(3,4-ethylenedioxythiophene):poly(styrenesulfonic acid), Heraeus Clevios] was deposited by spin-coating with a layer thickness of ~30 nm. Further processing was performed under nitrogen atmosphere in a glove box (<1 ppm O_2/H_2O), starting off with an annealing step at 130 °C for 15 min to remove any residual water. The photoactive layer solution, consisting of **P1**-**P6** and $PC_{71}BM$ (Solenne), was spin-coated from chlorobenzene. For a proper comparison, the optimal processing conditions for **P1** were used for all polymers. As such, a polymer:fullerene ratio of 1:4 (wt/wt) was used with a total concentration of 32 mg mL^{-1} and the solution was stirred overnight at 75 °C to ensure proper dissolution. The active layer was deposited on top of the PEDOT:PSS layer by means of spin-coating at room temperature with an optimal layer

thickness of 80-90 nm. In a final step, the top electrodes Ca (30 nm) and Al (80 nm) (or Au, 80 nm) were deposited by vacuum deposition to obtain complete solar cell (or hole-only) devices with an active area of 3 mm^2. The *J-V* characteristics of all photovoltaic devices were evaluated under AM1.5G solar illumination (100 mW cm^{-2}) using a Newport class A solar simulator (model 91195A), calibrated with a silicon solar cell. EQE measurements were performed with a Newport Apex illuminator (100 W Xenon lamp, 6257) as light source, a Newport Cornerstone 130° monochromator and a Stanford SR830 lock-in amplifier for the current measurements. A silicon FDS100-CAL photodiode was employed as a reference cell. AFM experiments were performed with a JPK NanoWizard 3 AFM (JPK Instruments AG, Berlin, Germany) using AC mode in air. Silicon ACTA-50 tips from AppNano with cantilever length ~125 mm, spring constant ~40 N m^{-1} and resonance frequency ~300 kHz were used. The scan angle, set point height, gain values and scan rate were adjusted according to the calibration of the AFM tip. TEM measurements were performed on a FEI Tecnai Spirit using an accelerating voltage of 120 kV.

Supporting Information

Supporting Information is available from the Wiley Online Library or from the author.

Acknowledgements: The calculations were performed on the computers of the Consortium des Équipements de Calcul Intensif (CECI, http://www.ceci-hpc.be), including those of the Technological Platform of High-Performance Computing, for which we gratefully acknowledge the financial support of the FNRS-FRFC (Conventions No. 2.4.617.07.F and 2.5020.11) and the University of Namur. The UHasselt co-authors thank Hasselt University and the Research Foundation – Flanders (FWO Vlaanderen) for continuous financial support and postdoctoral fellowships for JK and PV.

Keywords: donor-acceptor polymers, Stille cross-coupling, homocoupling, polymer solar cells

References

[1] L. Dou, J. You, Z. Hong, Z. Xu, G. Li, R. A. Street, Y. Yang, *Adv. Mater.* **2013**, *25*, 6642.

[2] K. A. Mazzio, C. K. Luscombe, *Chem. Soc. Rev.* **2015**, *44*, 78.

[3] Y. Liu, J. Zhao, Z. Li, C. Mu, W. Ma, H. Hu, K. Jiang, H. Lin, H. Ade, H. Yan, *Nat. Commun.* **2014**, *5*, 5293.

[4] G. Li, R. Zhu, Y. Yang, *Nat. Photonics* **2012**, *6*, 153.

[5] L. K. Jagadamma, M. Al-Senani, A. El-Labban, I. Gereige, G. O. Ngongang Ndjawa, J. C. D. Faria, T. Kim, K. Zhao, F. Cruciani, D. H. Anjum, M. A. McLachlan, P. M. Beaujuge, A. Amassian, *Adv. Energy Mater.* **2015**, *5*, 1500204.

[6] Z. He, B. Xiao, F. Liu, H. Wu, Y. Yang, S. Xiao, C. Wang, T. P. Russell, Y. Cao, *Nat. Photonics* **2015**, *9*, 174.

[7] Y. Lin, F. Zhao, Y. Wu, K. Chen, Y. Xia, G. Li, S. K. K. Prasad, J. Zhu, L. Huo, H. Bin, Z. G. Zhang, X. Guo, M. Zhang, Y. Sun, F. Gao, Z. Wei, W. Ma, C. Wang, J. Hodgkiss, Z. Bo, O. Inganäs, Y. Li, X. Zhan, *Adv. Mater.* **2016**, *29*, 1604155.

[8] W. Zhao, D. Qian, S. Zhang, S. Li, O. Inganäs, F. Gao, J. Hou, *Adv. Mater.* **2016**, *28*, 4734.

[9] D. Baran, T. Kirchartz, S. Wheeler, S. Dimitrov, M. Abdelsamie, J. Gorman, R. Ashraf, S. Holliday, A. Wadsworth, N. Gasparini, P. Kaienburg, H. Yan, A. Amassian, C. J.

Brabec, J. Durrant, I. McCulloch, *Energy Environ. Sci.* **2016**, *9*, 3783.

[10] D. Meng, D. Sun, C. Zhong, T. Liu, B. Fan, L. Huo, Y. Li, W. Jiang, H. Choi, T. Kim, J. Y. Kim, Y. Sun, Z. Wang, A. J. Heeger, *J. Am. Chem. Soc.* **2016**, *138*, 375.

[11] S. Holliday, R. S. Ashraf, A. Wadsworth, D. Baran, S. A. Yousaf, C. B. Nielsen, C.-H. Tan, S. D. Dimitrov, Z. Shang, N. Gasparini, M. Alamoudi, F. Laquai, C. J. Brabec, A. Salleo, J. R. Durrant, I. McCulloch, *Nat. Commun.* **2016**, *7*, 11585.

[12] W. Zhao, S. Li, H. Yao, S. Zhang, Y. Zhang, B. Yang, J. Hou, *J. Am. Chem. Soc.* **2017**, *139*, 7148.

[13] C. Amatore, E. Carré, A. Jutand, H. Tanaka, Q. Ren, S. Torii, *Chem. - A Eur. J.* **1996**, *2*, 957.

[14] A. L. Casado, J. A. Casares, P. Espinet, *Organometallics* **1997**, *16*, 5730.

[15] P. Espinet, A. M. Echavarren, *Angew. Chem. Int. Ed.* **2004**, *43*, 4704.

[16] B. Carsten, F. He, H. J. Son, T. Xu, L. Yu, *Chem. Rev.* **2011**, *111*, 1493.

[17] F. Lombeck, H. Komber, D. Fazzi, D. Nava, J. Kuhlmann, D. Stegerer, K. Strassel, J. Brandt, A. D. de Zerio Mendaza, C. Müller, W. Thiel, M. Caironi, R. Friend, M. Sommer, *Adv. Energy Mater.* **2016**, *6*, 1601232.

[18] P. Verstappen, I. Cardinaletti, T. Vangerven, W. Vanormelingen, F. Verstraeten, L. Lutsen, D. Vanderzande, J. Manca, W. Maes, *RSC Adv.* **2016**, *6*, 32298.

[19] T. Vangerven, P. Verstappen, N. Patil, J. D'Haen, I. Cardinaletti, J. Benduhn, N. Van den Brande, M. Defour, V. Lemaur, D. Beljonne, R. Lazzaroni, B. Champagne, K. Vandewal, J. W. Andreasen, P. Adriaensens, D. W. Breiby, B. Van Mele, D. Vanderzande, W. Maes, J. Manca, *Chem. Mater.* **2016**, *28*, 9088.

[20] L. Lu, T. Zheng, T. Xu, D. Zhao, L. Yu, *Chem. Mater.* **2015**, *27*, 537.

[21] T. Vangerven, P. Verstappen, J. Drijkoningen, W. Dierckx, S. Himmelberger, A. Salleo, D. Vanderzande, W. Maes, J. V. Manca, *Chem. Mater.* **2015**, *27*, 3726.

[22] K. H. Hendriks, W. Li, G. H. L. Heintges, G. W. P. Van Pruissen, M. M. Wienk, R. A. J. Janssen, *J. Am. Chem. Soc.* **2014**, *136*, 11128.

[23] F. Lombeck, R. Matsidik, H. Komber, M. Sommer, *Macromol. Rapid Commun.* **2015**, *36*, 231.

[24] G. Pirotte, P. Verstappen, D. Vanderzande, W. Maes, *Adv. Electron. Mater.* **2018**, 1700481.

[25] F. Lombeck, H. Komber, S. I. Gorelsky, M. Sommer, *ACS Macro Lett.* **2014**, *3*, 819.

[26] S. Broll, F. Nübling, A. Luzio, D. Lentzas, H. Komber, M. Caironi, M; Sommer, *Macromolecules* **2015**, *48*, 7481.

[27] P. Verstappen, J. Kesters, W. Vanormelingen, G. H. L. Heintges, J. Drijkoningen, T. Vangerven, L. Marin, S. Koudjina, B. Champagne, J. Manca, L. Lutsen, D. Vanderzande, W. Maes, *J. Mater. Chem. A* **2015**, *3*, 2960.

[28] P. Verstappen, J. Kesters, L. D. Olieslaeger, J. Drijkoningen, I. Cardinaletti, T. Vangerven, B. J. Bruijnaers, R. E. M. Willems, J. D. Haen, J. V Manca, L. Lutsen, D. J. M. Vanderzande, W. Maes, *Macromolecules* **2015**, *48*, 3873.

[29] A. E. Rudenko, B. C. Thompson, *J. Polym. Sci. Part A Polym. Chem.* **2015**, *53*, 135.

[30] H. Li, X. Qiao, W. Chen, Q. Wu, S. Zhang, H. Wu, Z. Liu, R. Yang, *Chem. Commun.* **2017**, *53*, 3543.

[31] F. Brouwer, J. Alma, H. Valkenier, T. P. Voortman, J. Hillebrand, R. C. Chiechi, J. C. Hummelen, *J. Mater. Chem.* **2011**, *21*, 1582.

[32] Y. Zhao, D. G. Truhlar, *Theor. Chem. Acc.* **2008**, *120*, 215.

[33] M. J. Frisch, G. W. Trucks, H. B. Schlegel, G. E. Scuseria, M. A. Robb, J. R. Cheeseman, G. Scalmani, V. Barone, B. Mennucci, G. A. Petersson, H. Nakatsuji, M. Caricato, X. Li, H. P. Hratchian, A. F. Izmaylov, J. Bloino, G. Zheng, J. L. Sonnenberg, M. Hada, M. Ehara, K. Toyota, R. Fukuda, J. Hasegawa, M. Ishida, T. Nakajima, Y. Honda, O. Kitao, H. Nakai, T. Vreven, J. A. Montgomery, Jr., J. E. Peralta, F. Ogliaro, M. Bearpark, J. J. Heyd, E. Brothers, K. N. Kudin, V. N. Staroverov, R. Kobayashi, J. Normand, K. Raghavachari, A. Rendell, J. C. Burant, S. S. Iyengar, J. Tomasi, M. Cossi, N. Rega, J. M. Millam, M. Klene, J. E. Knox, J. B. Cross, V. Bakken, C. Adamo, J. Jaramillo, R. Gomperts, R. E. Stratmann, O. Yazyev, A. J. Austin, R. Cammi, C. Pomelli, J. W. Ochterski, R. L. Martin, K. Morokuma, V. G. Zakrzewski, G. A. Voth, P. Salvador, J. J. Dannenberg, S. Dapprich, A. D. Daniels, Ö. Farkas, J. B. Foresman, J. V. Ortiz, J. Cioslowski, D. J. Fox, Gaussian-09 Revision D.01, Gaussian Inc. Wallingford CT **2009**.

[34] S. Wen, C. Wang, P. Ma, Y. Zhao, C. Li, S. Ruan, *J. Mater. Chem. A* **2015**, *3*, 13794.

[35] J. Bard, L. R. Faulkner, in *Electrochemical methods: fundamentals and applications, 2nd Ed.*, Wiley, **2001**.

[36] S. Trasatti, *Pure Appl. Chem.* **1986**, *58*, 955.

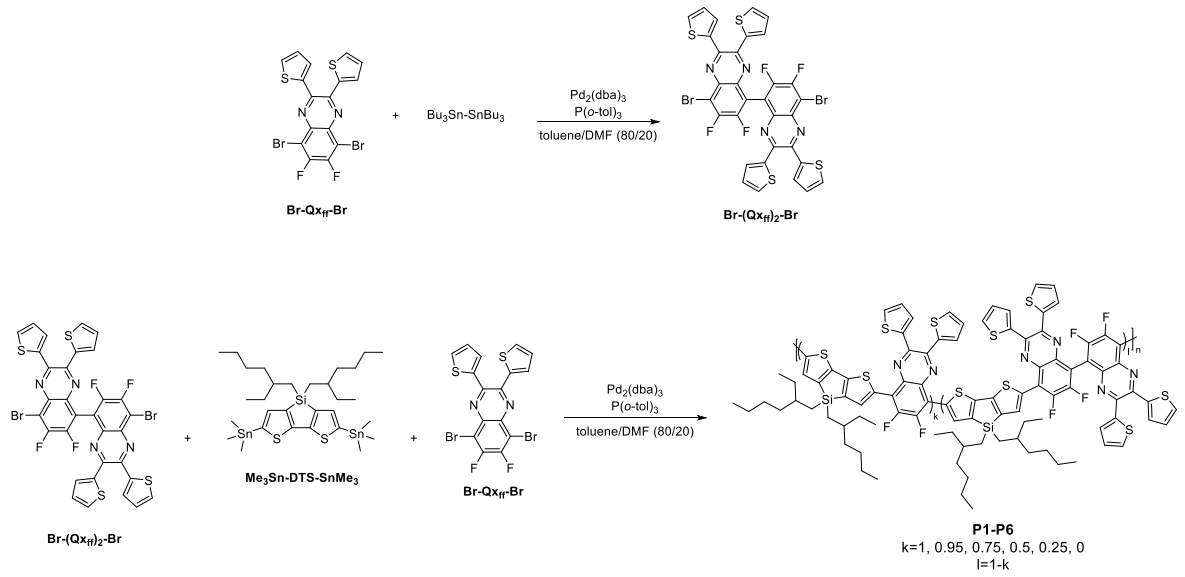

Scheme 1. Synthesis of the homocoupled quinoxaline monomer (top) and Stille polycondensation yielding the PDTSQx$_{ff}$ polymer series (**P1**-**P6**) with varying amounts of homocoupling (bottom).

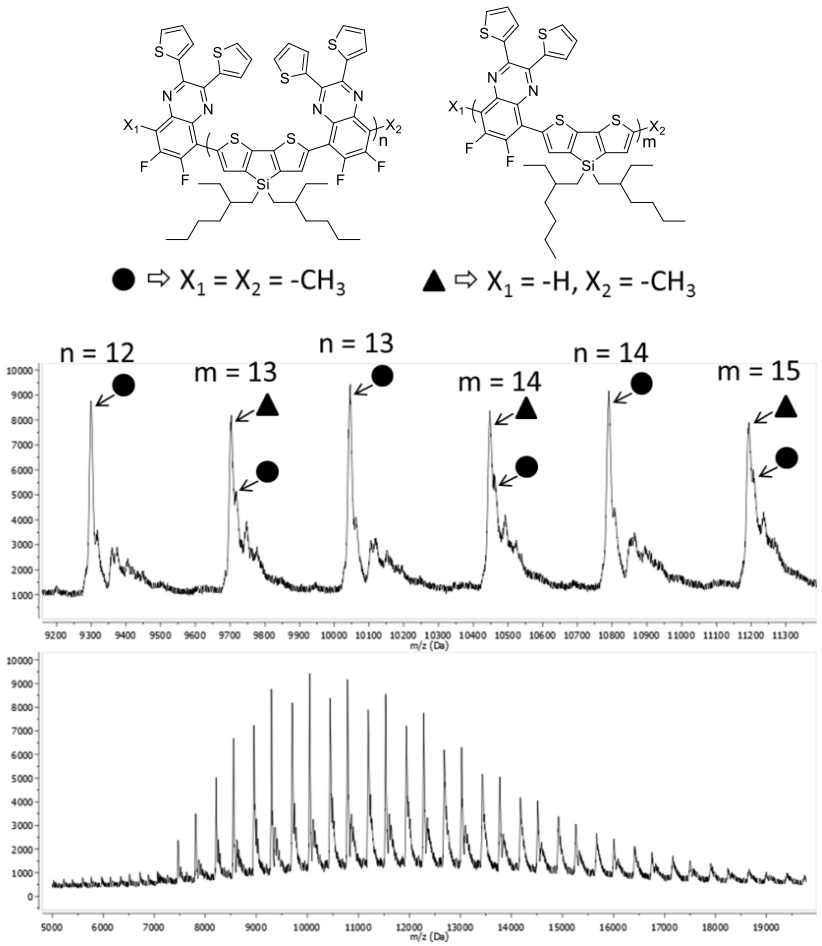

Figure 1. MALDI-TOF mass spectrum of the virtually defect-free PDTSQx$_{ff}$ polymer **P1**.

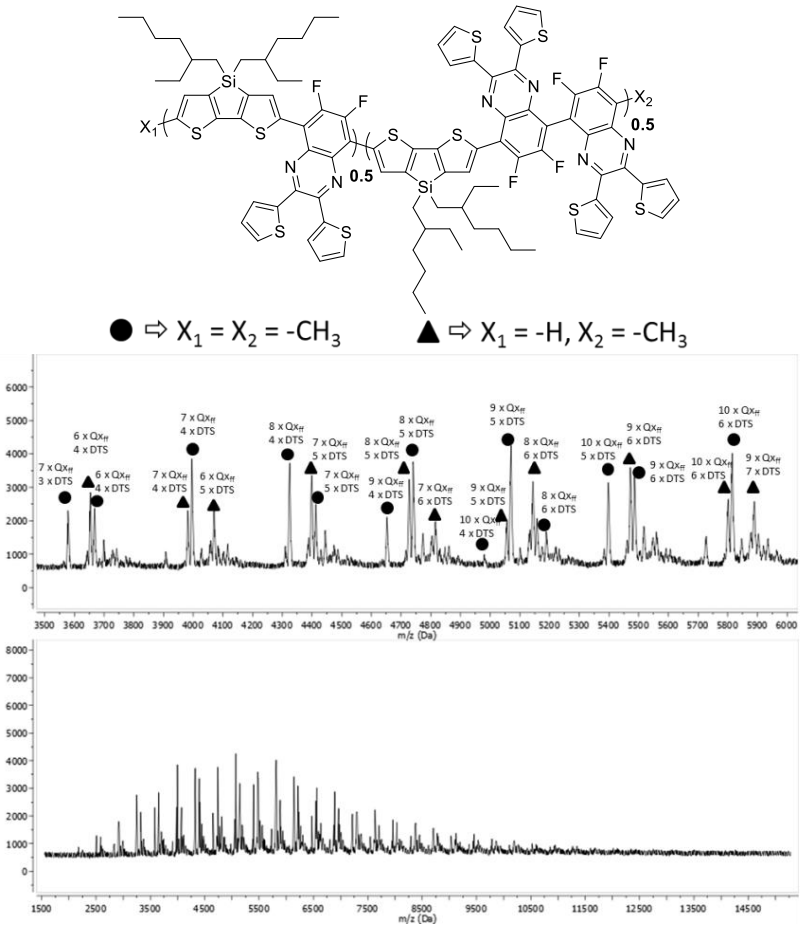

Figure 2. MALDI-TOF mass spectrum of lower molecular weight PDTSQx$_{ff}$ polymer **P4** with 50% homocoupling.

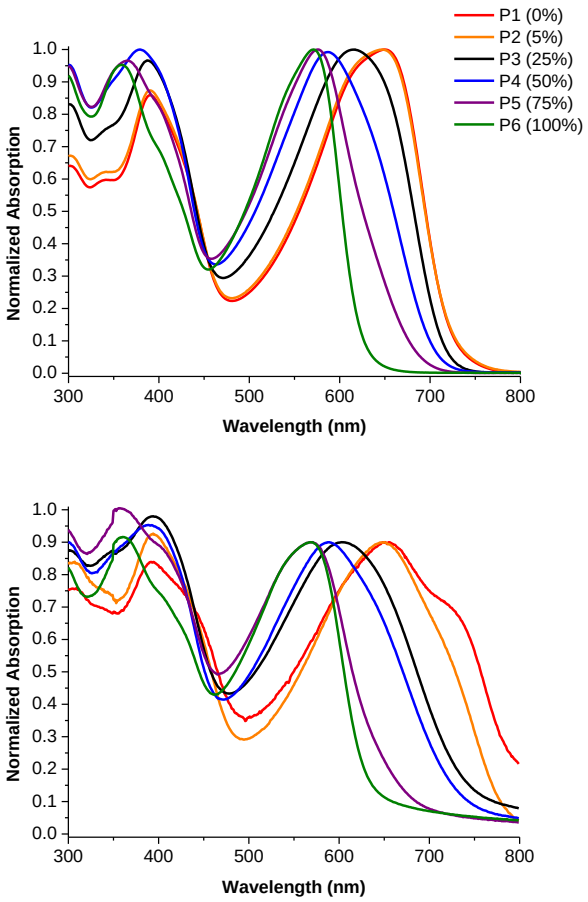

Figure 3. Normalized UV-VIS absorption spectra of polymers **P1**-**P6** in chloroform solution (top) and in thin film (bottom).

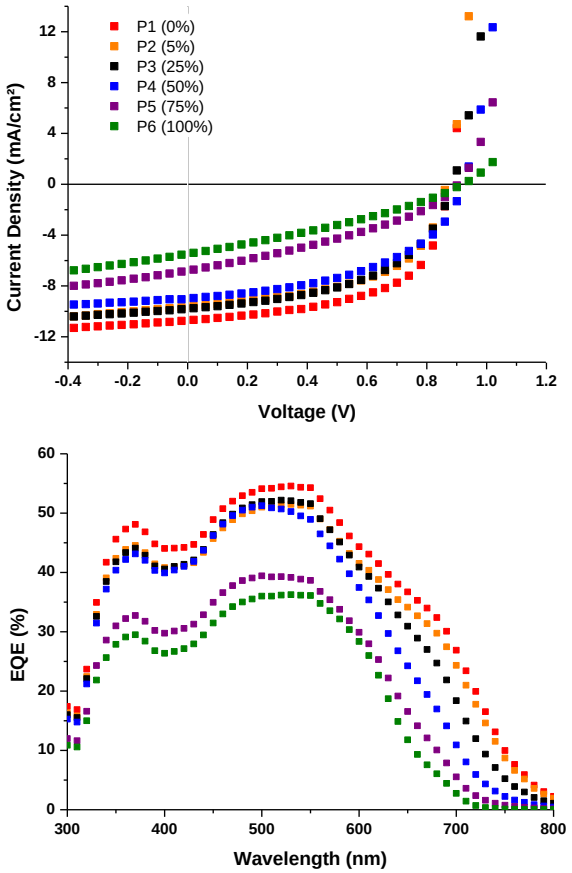

Figure 4. *J-V*-curves (top) and EQE spectra (bottom) of average performing photovoltaic devices incorporating **P1**-**P6**.

Table 1. Overview of the characterization data for PDTSQx$_{ff}$ polymers **P1**-**P6** with different homocoupling content.

Parameter	P1	P2	P3	P4	P5	P6
(Qx$_{ff}$)$_2$ [%]	0	5	25	50	75	100
M_n [kDa]	30.1	25.2	27.6	24.5	25.6	30.2
$Đ$	1.29	1.12	1.31	1.49	1.25	1.28
λ_{max} [nm][a)]	649 [630][b)]	647	617	587 [608][b)]	570	568 [577][b)]
ΔE_{opt} [eV]	1.65	1.68	1.66	1.68	1.89	1.95
ΔE_{EC} [eV]	2.09 [2.58][b)]	2.09	2.08	2.11 [2.65][b)]	2.20	2.28 [2.78][b)]
E_{ox} [V]	0.58	0.60	0.57	0.61	0.72	0.81
E_{red} [V]	-1.51	-1.49	-1.51	-1.51	-1.48	-1.47
E(HOMO) [eV]	-5.49 [-5.21][b)]	-5.51	-5.48	-5.51 [-5.29][b)]	-5.62	-5.71 [-5.41][b)]
E(LUMO) [eV]	-3.40 [-2.63][b)]	-3.42	-3.40	-3.40 [-2.64][b)]	-3.42	-3.43 [-2.63][b)]

[a)] Determined from UV-VIS absorption spectra of the polymer solutions in chloroform; [b)] Values in brackets are obtained using (TD)DFT calculations.

Table 2. Photovoltaic performances of BHJ polymer solar cells prepared from PDTSQx$_{ff}$ polymers **P1**-**P6** with different homocoupling content.

Active layer	**(Qx$_{ff}$)$_2$ [%]**	**V_{oc} [V]**	**J_{sc} [mA cm^{-2}]**	**FF**	**PCE$_{av}$ [%]**[a)]	**PCE$_{max}$ [%]**
P1/PC$_{71}$BM	0	0.86	10.51	0.59	5.35	5.62
P2/PC$_{71}$BM	5	0.86	9.83	0.56	4.73	5.02
P3/PC$_{71}$BM	25	0.89	9.43	0.54	4.56	4.81
P4/PC$_{71}$BM	50	0.91	8.61	0.47	3.70	4.02
P5/PC$_{71}$BM	75	0.90	6.65	0.35	2.12	2.21
P6/PC$_{71}$BM	100	0.91	5.23	0.31	1.50	1.70

[a)] Averages over at least 8 devices.

Table of contents entry

Homocoupling defects can strongly affect the optical and electronic properties of push-pull type conjugated polymers. This article focuses on the influence of homocoupling in the acceptor units on the material properties and final solar cell performance. To this extent, a specific ratio of homocoupled diquinoxaline moieties is introduced in the PDTSQx$_{ff}$ backbone.